American Mineralogist, Volume 84, pages 245–256, 1999

A new pyroxene structure at high pressure: Single-crystal X-ray and Raman study of the *Pbcn*-$P2_1cn$ phase transition in protopyroxene

Hexiong Yang,* Larry W. Finger, Pamela G. Conrad, Charles T. Prewitt, and Robert M. Hazen

Geophysical Laboratory and Center for High-Pressure Research, Carnegie Institution of Washington, 5251 Broad Branch Road, N.W., Washington, D.C. 20015-1305 U.S.A.

Abstract

The crystal structure of $(Mg_{1.54}Li_{0.23}Sc_{0.23})Si_2O_6$ protopyroxene has been studied with single-crystal X-ray diffraction at pressures to 9.98 GPa and Raman spectroscopy to 10.4 GPa. A first-order displacive phase transformation from the *Pbcn* space group to $P2_1cn$ was observed between 2.03 and 2.50 GPa, which is characterized by a discontinuous decrease in *a*, *c*, and *V* by 1.1, 2.4, and 2.6%, respectively, and an increase in *b* by 0.9%, along with appearance of intensities of some 0*kl* reflections with $k \neq 2n$. This is the first substantiated example of protopyroxene having the symmetry predicted by Thompson (1970). Evidence for the phase transition from Raman spectroscopy is also presented. The prominent structural changes associated with the *Pbcn*-to-$P2_1cn$ transformation involve the abrupt splitting of one type of O-rotated silicate chain in low-pressure protopyroxene into S-rotated A and O-rotated B chains in high-pressure protopyroxene, coupled with a marked decrease in the O3-O3-O3 angles and a re-configuration of O atoms around the M2 site. The kinking angle of the silicate chain in the low-pressure phase at 2.03 GPa is 165.9°, whereas the angles are 147.9° and 153.9° for the A and B chains, respectively, in high-pressure phase at 2.50 GPa. Strikingly, the two types of silicate chains in the $P2_1cn$ structure alternate along the *b* axis in a tetrahedral layer parallel to (100). Such a mixed arrangement of two differently rotated silicate chains in a tetrahedral layer has not been observed in any other pyroxene structure. Compression anisotropy of the protopyroxene structure is affected by the phase transition. The relative linear compressibilities (β_a:β_b:β_c) are 1.00:1.72:0.99 for low-pressure protopyroxene, but are 1.00:1.28:1.65 for high-pressure protopyroxene. The bulk moduli of low- and high-pressure phases are 130(3) and 111(1) GPa, respectively. This study concludes that the *Pbcn*-to-$P2_1cn$ phase transition results from the differential compression between SiO_4 tetrahedra and MO_6 octahedra.

Introduction

Silicate pyroxenes are important components in the Earth's crust, upper mantle, and meteorites (Ringwood 1975; Anderson 1989). A detailed knowledge of crystal structures and phase-transition mechanisms in pyroxenes is, therefore, of great geophysical importance in understanding the Earth's interior. Five Ca-poor pyroxene polymorphs are known: orthopyroxene, protopyroxene, low-clinopyroxene, high-clinopyroxene, and high-pressure clinopyroxene, with space groups *Pbca*, *Pbcn*, $P2_1/c$, $C2/c$, and $C2/c$, respectively. [Some inconsistencies exist in the nomenclature for high-temperature and high-pressure phases found in pyroxenes. Angel et al. (1992), Angel and Hugh-Jones (1994), and Hugh-Jones et al. (1997) called the high-pressure clinopyroxene phases ''high clinoenstatite'' and ''high clinoferrosilite,'' despite the fact that these two names were already used to refer to the high-temperature phases of clinopyroxenes. To avoid further confusion, only pyroxene phases found at high temperatures will be called ''high pyroxenes'' here and those found at high pressures called ''high-pressure pyroxenes.''] The crystal structures of various pyroxenes were thoroughly reviewed by Cameron and Papike (1981). All previously described pyroxene structures are characterized by single SiO_4 tetrahedral chains running parallel to the *c* axis; these chains are linked together along [100] by bands of octahedra occupied by two crystallographically distinct cations, M1 and M2. Viewed along the *c* axis, all pyroxene structures can be described in terms of different stacking sequences of alternating SiO_4 tetrahedral and MO_6 octahedral layers along *a**; all silicate chains in a tetrahedral layer are symmetrically related. The five polymorphs differ mainly in the configurations of the tetrahedral chains relative to the orientation of the octahedral bands.

Several high-pressure structure studies were performed on orthopyroxene, low-pressure clinopyroxene, and high-pressure clinopyroxene (Ralph and Ghose 1980; Angel et

* E-mail: yang@gl.ciw.edu

0003–004X/99/0003–0245$05.00

al. 1992; Hugh-Jones and Angel 1994; Hugh-Jones et al. 1994, 1996, 1997), but not on protopyroxene. Both orthopyroxene and low-pressure clinopyroxene transform to unquenchable high-pressure clinopyroxene at high pressures (e.g., Pacalo and Gasparik 1990; Angel et al. 1992; Hugh-Jones et al. 1994, 1996; Woodland and Angel 1997). Protopyroxene is the high-temperature stable form of Mg-rich orthopyroxene. Its crystal structure was first determined by Smith (1959, 1969) and refined using in-situ high-temperature data by Sadanaga et al. (1969), Smyth (1971), Murakami et al. (1984, 1985), and Yang and Ghose (1995a). Smyth and Ito (1975) found that Sc^{3+}, when coupled with Li^{+}, can stablize the protopyroxene structure at room temperature and refined the structure of a crystal with the composition $Mg_{1.4}Li_{0.3}Sc_{0.3}Si_2O_6$. The structure refinement of a Co-doped protopyroxene crystal ($Mg_{1.4}Co_{0.2}Li_{0.2}Sc_{0.2}Si_2O_6$) was reported by Murakami et al. (1985). In the protopyroxene structure, there is only one type of O-rotated silicate chain; of the two symmetrically nonequivalent octahedral sites, M1 is smaller and much less distorted than M2.

In the nearly 30 years since Thompson (1970) reviewed possible space-group symmetries of amphiboles and pyroxenes based on ideal close-packing of O atoms, many investigators have attempted to explain why the observed space groups of orthopyroxenes (*Pbca*) and protopyroxenes (*Pbcn*) do not correspond to the non-centrosymmetric space groups ($P2_1ca$ and $P2_1cn$) characteristic of the ideal structures (e.g., Papike et al. 1973). Some investigators did observe reflections in both orthopyroxene and protopyroxene diffraction patterns that appeared to violate the *b*-glide symmetry, but in virtually all cases these extra reflections could be ascribed to other causes such as multiple diffraction or the presence of an exsolved phase (Sasaki et al. 1984). This paper reports a systematic high-pressure structure study on protopyroxene by single-crystal X-ray diffraction to 9.98 GPa and Raman spectroscopy to 10.4 GPa. The *Pbcn* protopyroxene structure undergoes a reversible, displacive first-order transformation to a new pyroxene structure type with $P2_1cn$ symmetry at high pressure. This is the first substantiated example of a protopyroxene having the symmetry predicted by Thompson (1970).

Experimental procedures

Room-pressure X-ray diffraction data measurements

The protopyroxene sample used in this study was synthesized by the late Dr. Jun Ito and its chemical composition from microprobe analysis is $Mg_{1.54}Li_{0.23}Sc_{0.23}Si_2O_6$. The stability field of this phase in terms of composition and temperature was summarized by Takuchi (1997). A large single crystal was crushed into several small pieces from which two suitable fragments were selected: one (0.10 mm study × 0.09mm × 0.03 mm) showing sharp diffraction profiles for the single-crystal X-ray diffraction and the other (0.08 mm × 0.06 mm × 0.03 mm) for the Raman spectroscopy measurements. A Picker four-circle diffractometer equipped with a Mo X-ray tube (β-filtered) was used for all X-ray diffraction measurements. Unit-cell parameters were determined by fitting the positions of 16 reflections with $20° < 2\theta < 35°$ following the procedure of King and Finger (1979), yielding a = 9.2557(5), b = 8.7648(7), c = 5.3331(2) Å, and V = 432.64(4) Å^3.

X-ray diffraction intensity data from one quadrant of reciprocal space with $0° \leq 2\theta \leq 60°$ were collected on the basis of the primitive lattice using ω scans of 1° width in step increments of 0.025° and 2-s per step counting time. Digitized step data were integrated by the method of Lehmann and Larsen (1974) with background manually reset when necessary. Corrections were made for Lorentz and polarization effects and for X-ray absorption by the crystal (μ = 13.76 cm^{-1}). Reflections having intensities greater than $2\sigma(I)$ were considered as observed and included in the refinement, where $\sigma(I)$ is the standard deviation determined from the counting statistics. The total number of observed reflections was 1102, out of which 581 reflections were symmetry-independent after averaging in Laue group *mmm* (R_{int} = 0.009). No reflections violating the space group *Pbcn* were found.

The initial structural model of protopyroxene was taken from Smyth and Ito (1975). Least-squares refinements were carried out using an updated version of RFINE4 (Finger and Prince 1975) in the *Pbcn* space group. Neutral atomic scattering factors, including anomalous dispersion corrections for Mg, Li, Sc, Si, and O, were taken from Ibers and Hamilton (1974). Weighting schemes were based on $w = [\sigma^2(F) + (pF)^2]^{-1}$ where p was adjusted to ensure that the errors were normally distributed through probability plot analysis (Ibers and Hamilton 1974). Type II isotropic extinction corrections (Becker and Coppens 1975) were applied in the refinements. The refinement without the compositional constraint showed that all Sc was ordered in M1 with a site occupancy of 0.228(3) and Li in M2 with a site occupancy of 0.236(4), in good agreement with the microprobe analysis result. Thus, both Sc and Li were fixed to be 0.23 in M1 and M2, respectively, in the final refinement, which gave R_w = 0.018 and R = 0.017. Atomic positional coordinates and anisotropic displacement parameters at room pressure are available upon request.

High-pressure X-ray diffraction data measurements

After collection of X-ray intensity data at room pressure, the same crystal was mounted in a modified Merrill-Bassett diamond-anvil cell with a mixture of 4:1 methanol:ethanol as the pressure medium. Four ruby chips (<10 μm) were included as the internal pressure calibrant (Mao et al. 1986), from which pressure was determined from the position of the R_1 laser-induced fluorescence peak with an error of approximately 0.05 GPa. The fixed-ϕ mode of data measurement (Finger and King 1978) was used throughout the high-pressure experiments to maximize reflection accessibility and minimize attenuation by the diamond cell. Lattice parameters were determined us-

TABLE 1. Crystal data and other relevant information on protopyroxene at various pressures

P (GPa)	*a* (Å)	*b* (Å)	*c* (Å)	*V* (Å^3)	Refls. > $2\sigma_I$	R_{int}*	R_w†	*R*‡	Space Group
0.00	9.2554(4)	8.7650(5)	5.3333(2)	432.65(3)	262	0.028	0.029	0.036	*Pbcn*
1.11	9.2351(4)	8.7310(5)	5.3216(2)	429.09(2)	253	0.027	0.027	0.034	*Pbcn*
2.03	9.2178(6)	8.7039(6)	5.3119(4)	426.16(4)	245	0.031	0.029	0.036	*Pbcn*
2.50	9.1167(4)	8.7857(4)	5.1837(2)	415.19(3)	250	0.035	0.020	0.030	$P2_1cn$
4.22	9.0877(5)	8.7526(5)	5.1531(3)	409.89(3)	267	0.032	0.022	0.031	$P2_1cn$
6.14	9.0548(6)	8.7120(6)	5.1209(3)	403.97(4)	276	0.029	0.022	0.031	$P2_1cn$
7.93	9.0219(7)	8.6711(6)	5.0898(4)	398.18(5)	276	0.026	0.025	0.033	$P2_1cn$
9.98	8.9921(8)	8.6310(7)	5.0659(5)	393.17(6)	264	0.025	0.026	0.034	$P2_1cn$

* Residual for internal agreement of symmetry equivalent reflections.
† $R_w = (\Sigma w(F_o - F_c)^2/\Sigma wF_o^2)^{0.5}$.
‡ $R = \Sigma|F_o - F_c|/\Sigma|F_o|$.

ing the same method as described for the room-pressure experiment.

As pressure was increased from 2.03 to 2.50 GPa, a significant change occurred in all unit-cell dimensions (Table 1) and intensities of some reflections, indicating that a phase transition had taken place within this pressure range. The crystal quality was then checked carefully by examining peak profiles of reflection data collected at 2.50 GPa; no significant peak broadening was observed for all reflections. In addition, examination of X-ray intensity data collected at this pressure revealed the presence of 0*kl* reflections with $k \neq 2n$ (which will be called the b-type reflections hereafter), suggesting that the *Pbcn* symmetry of protopyroxene had been violated, and the crystal had transformed to a new structure with the possible space group $P2_1cn$ or *Pmcn*. The structure of the high-pressure phase was solved based on the space group $P2_1cn$ using direct methods (SHELX-97. The low-pressure phase will be refered to hereafter as low-*P* protopyroxene and the high-pressure phase as high-*P* protopyroxene. After the data collection at 6.14 GPa, the pressure of the crystal was gradually released to check the reversibility of the phase transition; the low-*P* protopyroxene unit cell was recovered when pressure was lowered from 1.55 to 1.30 GPa, accompanied by the disappearance of all b-type reflections. The pressure of the crystal was then raised again to collect data at 7.93 and 9.98 GPa.

X-ray diffraction intensity data were collected for all accessible reflections with $0° \leq 2\theta \leq 60°$. For better comparison with high-pressure data, another set of room-pressure intensity data were collected with the crystal mounted in the diamond-anvil cell. The experimental procedures for data collection, reduction, and structure refinements were similar to those described above for the data collected at room pressure, but only atomic isotropic displacement factors were refined for high-*P* protopyroxene. In addition, corrections were made for absorption by the diamond and beryllium components of the pressure cell. For all high-pressure structure refinements, the Li-Sc distribution between the M1 and M2 sites was assumed to be the same as that for the refinement with the data collected without the diamond-anvil cell. Unit-cell dimensions and final refinement statistics are in Table 1; atomic positional and isotropic displacement parameters are in Table 2; selected interatomic distances; angles are in Table 3 and polyhedral volumes and distortion indices are in Table 4.

High-pressure Raman spectroscopy

Unpolarized Raman spectra were collected from a single crystal of $(Mg_{1.54}Li_{0.23}Sc_{0.23})Si_2O_6$ protopyroxene at a series of pressures from ambient to 10.4 GPa in a diamond-anvil cell at room temperature. Pressure was calibrated by grains of ruby positioned symmetrically about the protopyroxene crystal in a methanol-ethanol-water (16:4:1) pressure medium. A 514.5 nm argon ion laser operating at 400 mW power was used to excite optical phonons in a tabular crystal, approximately normal to the *c* crystallographic axis. A 50× microscope objective was used to focus the laser on the crystal; the scattered light was collected through the same objective (a 180° backscattering angle) and directed by mirrors through a focusing lens and into the slit of a Spex spectrometer with movable grating and CCD detector. Data from the multichannel analyzer (1024 channels) were accessed via Winspec software. No evidence of heating was observed.

RESULTS AND DISCUSSION

Variations of unit-cell parameters with pressure

The *Pbcn*-$P2_1cn$ phase transition in protopyroxene between 2.03 and 2.50 GPa was marked by a discontinuity in all unit-cell parameters (Fig. 1): *a*, *c*, and *V* decreased by 1.1, 2.4, and 2.6%, respectively, whereas *b* increased by 0.9%. A similar change in unit-cell dimensions was observed in the transformation from low- to high-*P* clinoenstatite at high pressure (Angel and Hugh-Jones 1994). Such a change should also be compared to that associated with the orthoenstatite-to-protoenstatite phase transition at high temperatures in which *a* and *c* abruptly increase and *b* decreases (Yang and Ghose 1995a). Considering the commonly inverse effects of temperature and pressure on crystal structures (Hazen and Finger 1982), the similarity in unit-cell parameter changes across different phase transitions suggests a similar mechanism of structural modification. Within experimental uncertainties, all unit-cell di-

TABLE 2. Atomic positional coordinates and isotropic displacement parameters of protopyroxene at various pressures

P (GPa)	0.00	1.11	2.03	2.50	4.22	6.14	7.93	9.98
M1 *x*	0	0	0	0	0	0	0	0
M1 *y*	0.0983(2)	0.0979(2)	0.0976(2)	0.0990(2)	0.0986(2)	0.0979(2)	0.0977(2)	0.0968(3)
M1 *z*	0.75	0.75	0.75	0.7190(3)	0.7161(3)	0.7133(3)	0.7105(4)	0.7087(4)
M1 *B*	0.54(3)	0.55(3)	0.60(3)	0.54(3)	0.52(3)	0.51(3)	0.58(3)	0.51(4)
M2 *x*	0	0	0	0.0061(6)	0.0086(5)	0.0104(5)	0.0120(5)	0.0127(5)
M2 *y*	0.2644(3)	0.2654(3)	0.2656(4)	0.2630(3)	0.2645(3)	0.2652(3)	0.2666(3)	0.2664(4)
M2 *z*	0.25	0.25	0.25	0.2183(5)	0.2151(5)	0.2116(5)	0.2103(6)	0.2090(6)
M2 *B*	0.73(5)	0.70(5)	0.74(5)	0.71(5)	0.65(5)	0.65(5)	0.74(5)	0.68(6)
SiA *x*				0.7019(4)	0.7016(4)	0.7022(4)	0.7021(4)	0.7016(5)
SiA *y*				0.9111(3)	0.9106(3)	0.9103(3)	0.9104(3)	0.9101(3)
SiA *z*				0.8700(3)	0.8651(3)	0.8608(3)	0.8567(3)	0.8545(4)
SiA *B*				0.39(3)	0.38(3)	0.40(3)	0.43(3)	0.44(4)
SiB *x*	0.2931(1)	0.2930(1)	0.2930(2)	0.2987(4)	0.2992(4)	0.3002(4)	0.3001(4)	0.3006(5)
SiB *y*	0.0904(1)	0.0907(1)	0.0908(2)	0.0876(3)	0.0876(3)	0.0880(3)	0.0886(3)	0.0884(3)
SiB *z*	0.0731(2)	0.0738(2)	0.0743(2)	0.0702(3)	0.0699(3)	0.0688(3)	0.0682(3)	0.0669(3)
SiB *B*	0.49(3)	0.48(2)	0.49(3)	0.43(3)	0.40(3)	0.36(3)	0.45(3)	0.38(4)
O1A *x*				0.8801(7)	0.8794(7)	0.8805(7)	0.8806(7)	0.8797(8)
O1A *y*				0.9100(8)	0.9112(8)	0.9094(7)	0.9093(7)	0.9104(8)
O1A *z*				0.8815(7)	0.8777(7)	0.8741(7)	0.8718(8)	0.8692(9)
O1A *B*				0.51(9)	0.57(8)	0.40(8)	0.32(9)	0.58(10)
O1B *x*	0.1189(3)	0.1191(3)	0.1187(3)	0.1238(7)	0.1242(7)	0.1243(7)	0.1234(7)	0.1227(8)
O1B *y*	0.0920(4)	0.0921(4)	0.0921(4)	0.0864(9)	0.0862(9)	0.0846(9)	0.0841(8)	0.0833(9)
O1B *z*	0.0799(5)	0.0807(5)	0.0800(6)	0.0591(8)	0.0570(8)	0.0557(8)	0.0547(9)	0.0540(9)
O1B *B*	0.50(5)	0.51(5)	0.61(6)	0.47(9)	0.41(8)	0.46(8)	0.46(9)	0.46(10)
O2A *x*				0.6227(7)	0.6228(7)	0.6244(6)	0.6241(7)	0.6239(7)
O2A *y*				0.7585(8)	0.7589(8)	0.7596(8)	0.7594(8)	0.7605(9)
O2A *z*				0.9578(8)	0.9590(8)	0.9598(8)	0.9614(8)	0.9623(9)
O2A *B*				0.63(9)	0.63(9)	0.39(9)	0.48(9)	0.37(10)
O2B *x*	0.3749(3)	0.3744(3)	0.3740(3)	0.3756(8)	0.376(7)	0.3757(7)	0.3758(8)	0.3741(8)
O2B *y*	0.2493(4)	0.2510(4)	0.2509(4)	0.2468(7)	0.2470(7)	0.2497(8)	0.2489(7)	0.2498(8)
O2B *z*	0.0702(5)	0.0711(5)	0.0728(6)	0.1015(8)	0.1034(8)	0.1063(8)	0.1104(9)	0.1109(9)
O2B *B*	0.79(6)	0.76(6)	0.78(6)	0.77(9)	0.74(9)	0.76(9)	0.68(10)	0.69(10)
O3A *x*				0.6463(6)	0.6447(6)	0.6468(6)	0.6436(7)	0.6435(7)
O3A *y*				0.9576(6)	0.9534(6)	0.9512(7)	0.9478(7)	0.9455(8)
O3A *z*				0.5788(8)	0.5701(8)	0.5615(8)	0.5548(9)	0.5517(9)
O3A *B*				0.80(9)	0.79(9)	0.77(9)	0.56(10)	0.60(10)
O3B *x*	0.3499(3)	0.3503(3)	0.3509(4)	0.3581(6)	0.3587(5)	0.3615(6)	0.3617(7)	0.3633(7)
O3B *y*	0.9816(4)	0.9813(4)	0.9811(5)	0.9659(6)	0.9653(6)	0.9617(6)	0.9593(6)	0.9576(7)
O3B *z*	0.3023(5)	0.3048(4)	0.3051(6)	0.2802(7)	0.2781(7)	0.2758(8)	0.2741(8)	0.2719(9)
O3B *B*	0.60(6)	0.62(6)	0.64(6)	0.32(9)	0.42(9)	0.27(8)	0.47(9)	0.29(10)

Note: The *x* coordinate of M1 for high-pressure protopyroxene was fixed at zero and not varied. The origin of the $P2_1cn$ space group, as defined in *International Tables for Crystallography,* was translated by 1/4 *b* so that the coordinates in *Pbcn* and $P2_1cn$ space groups could be compared. The resulting symmetry transformations for $P2_1cn$ are *x, y, z;* 1/2 + *x,* 1/2-*y, -z;* 1/2 + *x,* 1/2 + *y,* 1/2-*z; x,-y,* 1/2 + *z.*

mensions of both low- and high-*P* protopyroxenes vary linearly with pressure. Both phases display rather strong compression anisotropy but with a change in the most compressible direction across the phase transition. In low-*P* protopyroxene, the *b* dimension is ~72% more compressible than *a* or *c*, whereas the *c* dimension becomes the most compressible in high-*P* protopyroxene. The respective linear compressibilities of the *a*, *b*, and *c* dimensions are 0.00200(2), 0.00344(4), and 0.00198(1) GPa^{-1} for low-*P* protopyroxene with β_a: β_b: β_c = 1.00:1.72:0.99 and 0.00184(4), 0.00237(4), and 0.00306(13) GPa^{-1} for high-*P* protopyroxene with β_a: β_b: β_c = 1.00:1.28:1.65. The increase in β_c at the transition appears coupled with the decrease in β_b. From Brillouin scattering measurements at ambient conditions on a *Pbcn* protopyroxene crystal with the composition $(Mg_{1.6}Li_{0.2}Sc_{0.2})Si_2O_6$, Vaughan and Bass (1983) also found that the structure is the softest along the *b* axis. The softest directions in orthoenstatite and clinoenstatite are along the *b* dimension as well (Weidner et al. 1978; Hugh-Jones and Angel 1994; Angel and Hugh-Jones 1994).

Weighted volume and pressure data fit to a second-order Birch-Murnahan equation of state produces V_0 = 432.65(5) Å^3 and bulk modulus K_0 = 130(3) GPa (with $\partial K/\partial P = K' \equiv 4$) for low-*P* protopyroxene and V_0 = 424.4(2) Å^3 and K_0 = 11(1) GPa ($K' \equiv 4$) for high-*P* protopyroxene. The larger compressibility of the high-pressure $P2_1cn$ structure compared to the low-pressure form is typical of some polyhedral tilt phase transitions in which the lower symmetry, high-pressure form has a

TABLE 3. Selected interatomic distances (Å) and angles (°) for protopyroxene at various pressures

P (GPa)	0.00	1.11	2.03	2.50	4.22	6.14	7.93	9.98
M1-O1A	2.195 (4)*	2.185(4)*	2.177(4)*	2.064(5)	2.061(5)	2.047(5)	2.034(5)	2.033(6)
M1-O1A′				2.159(7)	2.141(7)	2.132(6)	2.122(6)	2.102(7)
M1-O1B	2.076(3)*	2.076(3)*	2.067(3)*	2.096(5)	2.091(5)	2.087(5)	2.079(5)	2.071(6)
M1-O1B′				2.148(7)	2.136(7)	2.109(7)	2.086(7)	2.061(8)
M1-02A	2.011(3)*	1.998(3)*	1.993(3)*	2.014(7)	2.007(7)	2.010(6)	1.996(7)	1.997(7)
M1-O2B				1.997(6)	1.990(6)	1.970(6)	1.964(6)	1.965(7)
Average	2.093	2.086	2.079	2.080	2.071	2.059	2.047	2.038
M2-O1A	2.078(4)*	2.076(4)*	2.072(4)*	2.085(7)	2.109(7)	2.095(7)	2.099(7)	2.102(8)
M2-O1B				2.059(8)	2.050(8)	2.044(8)	2.035(7)	2.023(9)
M2-O2A	2.067(3)*	2.070(3)*	2.076(3)*	1.988(6)	1.975(6)	1.975(6)	1.954(6)	1.943(6)
M2-O2B				2.042(7)	2.039(6)	2.038(6)	2.047(7)	2.049(7)
M2-O3A	2.373(4)*	2.356(4)*	2.344(5)*	2.632(6)	2.534(6)	2.471(6)	2.387(7)	2.349(7)
M2-O3B				2.235(6)	2.224(6)	2.180(6)	2.153(7)	2.130(7)
Average	2.172	2.167	2.164	2.173	2.155	2.134	2.113	2.099
SiB-O1A	1.613(3)	1.607(3)	1.607(3)	1.626(7)	1.617(7)	1.616(7)	1.612(7)	1.603(9)
SiB-O2A	1.585(4)	1.589(4)	1.581(4)	1.589(7)	1.584(7)	1.574(7)	1.579(7)	1.566(8)
SiB-O3A	1.637(3)	1.644(3)	1.643(4)	1.661(5)	1.673(5)	1.663(6)	1.675(6)	1.681(7)
SiB-O3A′	1.661(3)	1.651(3)	1.650(4)	1.644(5)	1.649(5)	1.652(5)	1.657(5)	1.649(6)
Average	1.624	1.623	1.620	1.630	1.631	1.626	1.631	1.625
SiA-O1B				1.596(7)	1.592(7)	1.594(7)	1.596(7)	1.602(9)
SiA-O2B				1.573(7)	1.569(7)	1.578(7)	1.564(7)	1.561(8)
SiA-O3B				1.620(5)	1.609(5)	1.626(5)	1.632(6)	1.634(6)
SiA-O3B′				1.665(4)	1.664(4)	1.657(5)	1.650(5)	1.646(5)
Average				1.613	1.609	1.614	1.610	1.611
O3A-O3A-O3A	166.2(3)	166.0(3)	165.9(4)	147.9(4)	144.9(4)	143.3(5)	140.8(5)	139.3(6)
O3B-O3B-O3B				153.9(4)	153.5(4)	150.8(4)	149.0(4)	147.8(5)

* These bond distances have the multiplicity of 2.

greater number of tilting degrees of freedom (Hazen and Finger 1979, 1984). The bulk modulus determined for low-protopyroxene was slightly greater than 114 GPa measured by Vaughan and Bass (1983) using Brillouin scattering. The discrepancy could also result from the fact that $K' = 4$ was assumed for the data fitting, due to the limited data sets for the low-*P* phase or from the larger Sc content (by 3%) in the sample. Comparing bulk moduli for protopyroxenes with those for other enstatite polymorphs, Weidner et al. (1978) reported a bulk modulus of 107(3) GPa for orthoenstatite, whereas Hugh-Jones and Angel (1994) found $K_T = 96(3)$ GPa for $P < 4$ GPa and 123(17) GPa for $P > 4$ GPa. K_T of low- and high-*P* clinoenstatites are 111(3) and 104(6) GPa, respectively (Angel and Hugh-Jones 1994). Thus, given experimental uncertainties, structural differences among enstatite polymorphs do not significantly influence compressibilities.

Structural variations of low-*P* protopyroxene with pressure

The crystal structure of low-*P* protopyroxene contains only one type of crystallographically distinct silicate chain. Among all five enstatite-related polymorphs, low-*P* protopyroxene shows the least deviation of the O3-O3-O3 angle from 180° and the least compressibility along the *c* direction. Combining this data with those for orthoenstatite and clinoenstatite (Angel and Hugh-Jones 1994; Hugh-Jones and Angel 1994) showed that a larger β_c value is associated with the more kinked silicate chains in pyroxenes. A similar observation has been made by Vaughan and Bass (1983) from comparison of Brillouin scattering data for protoenstatite and orthoenstatite. Between room pressure and 2.03 GPa, the O3-O3-O3 angle in low-*P* protopyroxene does not decrease significantly (Table 4), but the O3-O3 distance within the SiO_4 tetrahedron shortens by 0.4%. No obvious variation was observed in the volume or distortion indices of the SiO_4 tetrahedron as a function of pressure.

In low-*P* protopyroxene, the M2 octahedron is extremely distorted from sharing two O2-O3 edges with the adjacent silicate chains. Due to high distortion, the volume of the M2 octahedron was smaller than that of the M1 octahedron, despite the fact that the mean M2-O bond distance was longer than the mean M1-O distance. Unlike the SiO_4 tetrahedron, the geometries of the M1 and M2 octahedra strongly depend on pressure. Up to 2.03 GPa, the M1 octahedron became slightly less distorted (Table 4) in terms of quadratic elongation and angle variance (*AV*) (Robinson et al. 1971), and all individual M-O bond lengths within the M1 octahedron decreased, yielding a 0.7% reduction in the mean M1-O distance. In contrast, the M2 octahedron became progressively more distorted with raised pressure and had an *AV* value of 342.9 at 2.03 GPa. Up to 2.03 GPa, the longest M2-O3 distance within the M2 octahedron shortened considerably from 2.373(4) to 2.344(5) Å, whereas the two short M2-O1 and M2-O2 lengths remained essentially constant (Fig. 2); the mean M2-O bond distance compressed by 0.4% within this pressure range. The significant shortening of the M2-O3 distances was accompanied by reduction of the M2-Si separation from 2.873(2) Å at room pressure to 2.858(2)

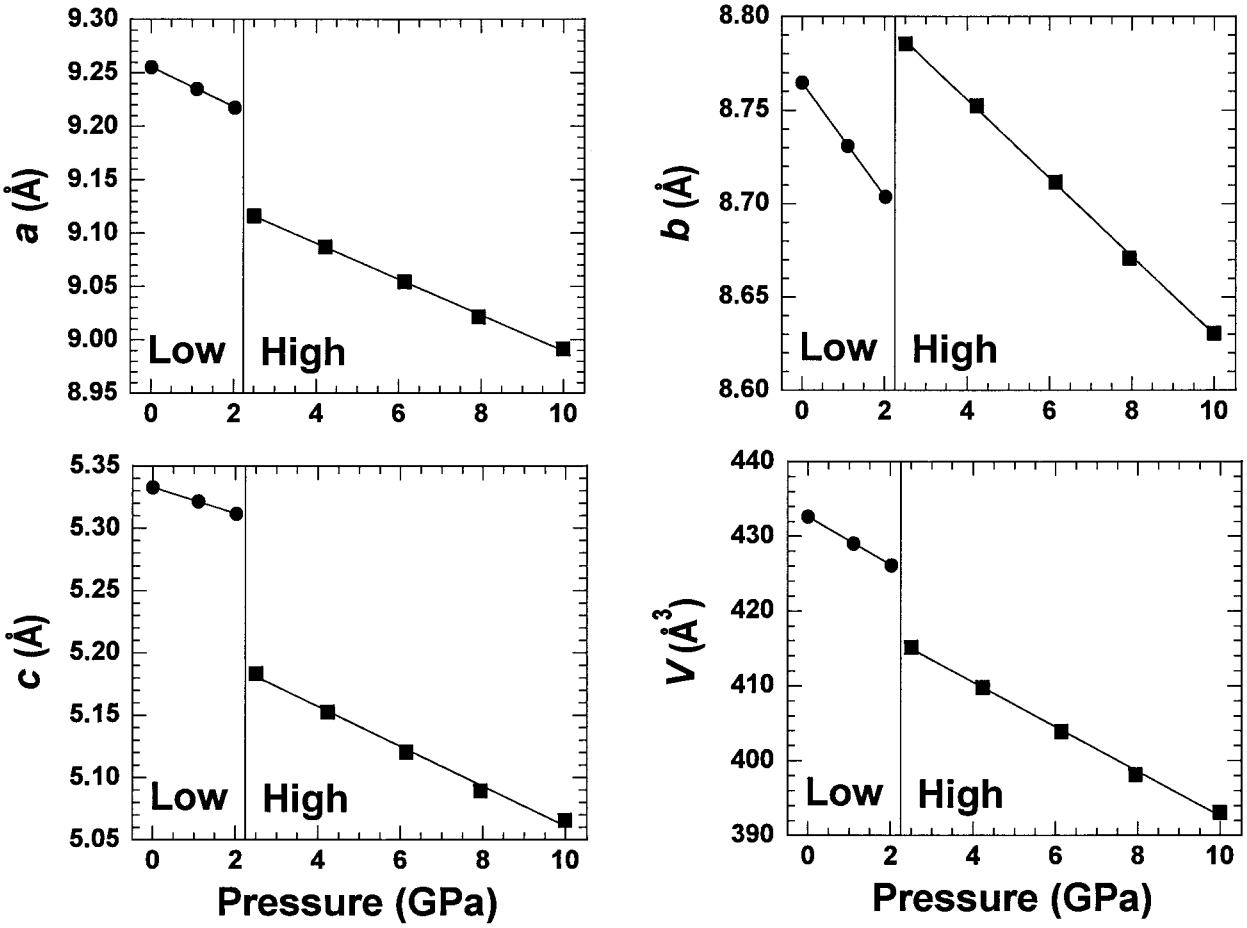

FIGURE 1. Variations of unit-cell parameters of protopyroxene with pressure. Abbreviations: Low = low-*P* protopyroxene and High = high-*P* protopyroxene.

Å at 2.03 GPa. The bulk moduli of the M1 and M2 octahedra were 99(22) and 121(10) GPa, respectively.

Structural variations of high-P protopyroxene with pressure

As in other pyroxene polymorphs, two crystallographically distinct octahedral sites, M1 and M2, exist in high-*P* protopyroxene. However, high-*P* protopyroxene differs in that it contains two symmetrically nonequivalent tetrahedral chains—an S-rotated A and an O-rotated B chain (Fig. 3)—resulting from the loss of *b*-glide symmetry. These two types of silicate chains occurred alternately along the *b* axis in a tetrahedral layer parallel to (100) (Fig. 4). Such a mixed arrangement of two differently

TABLE 4. Polyhedral volumes (Å^3) and distortion indices for protopyroxene at various pressures

P (GPa)	0.00	1.11	2.03	2.50	4.22	6.14	7.93	9.98
M1 *V**	12.07(2)	11.98(3)	11.82(2)	11.86(4)	11.72(4)	11.52(4)	11.32(4)	11.18(4)
M1 *QE*	1.0108(2)	1.0104(3)	1.0103(2)	1.0086(3)	1.0079(3)	1.0077(3)	1.0077(3)	1.0070(3)
M1 *AV*	32.8(3)	31.5(3)	31.2(3)	26.8(5)	24.8(5)	24.1(5)	24.0(5)	22.3(5)
M2 *V*	11.34(2)	11.25(3)	11.15(2)	12.87(4)	12.59(4)	12.31(4)	11.96(4)	11.76(4)
M2 *QE*	1.1380(6)	1.1403(7)	1.1402(7)	1.0523(6)	1.0471(6)	1.0408(6)	1.0386(6)	1.0363(7)
M2 *AV*	332.5(6)	339.0(7)	342.9(8)	131.9(9)	125.3(9)	112.2(9)	112.7(9)	107.1(9)
SiA *V*	2.17(1)	2.16(1)	2.16(1)	2.13(1)	2.12(1)	2.13(1)	2.12(1)	2.12(1)
SiA *QE*	1.0085(2)	1.0080(3)	1.0081(3)	1.0069(4)	1.0069(4)	1.0071(4)	1.0075(4)	1.0072(5)
SiA *AV*	33.8(5)	31.8(6)	32.0(5)	27.3(8)	27.4(8)	28.3(8)	29.5(9)	27.8(9)
SiB *V*				2.21(1)	2.21(1)	2.20(1)	2.22(1)	2.19(1)
SiB *QE*				1.0036(3)	1.0039(4)	1.0033(3)	1.0033(3)	1.0037(4)
SiB *AV*				14.1(7)	14.9(7)	12.3(6)	12.0(6)	13.3(7)

* *V* = polyhedral volume; *QE* = polyhedral quadratic elongation; *AV* = polyhedral angle variance (Robinson et al. 1971).

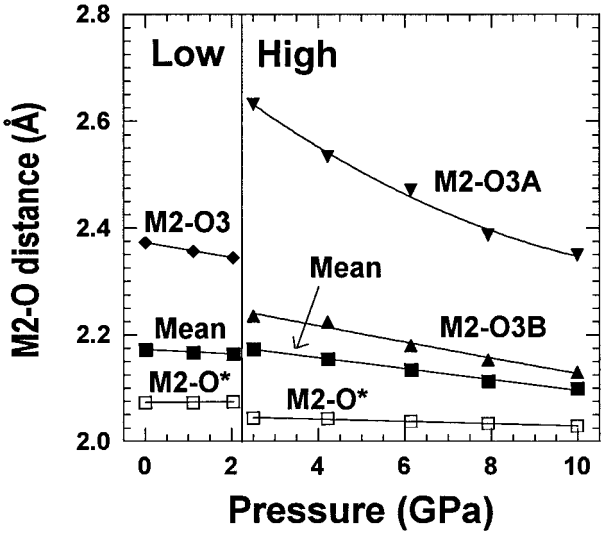

FIGURE 2. Variations of M2-O bond lengths with pressure. M2-O* represents the average of four short M2-O1 and M2-O2 bond lengths within the M2 octahedron.

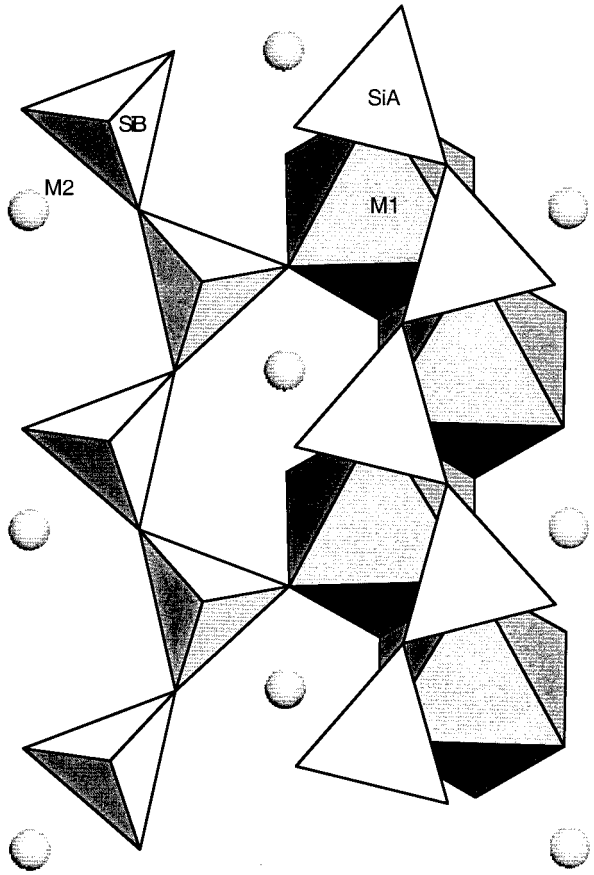

FIGURE 3. Projection of the high-pressure protopyroxene structure at 2.50 GPa along [100]. Note, the S-rotated chain is designated as the A chain to follow the convention for $P2_1/c$ clinopyroxene. The triangular faces of the SiA tetrahedra in Figure 3 are oriented approximately in the same (S) direction as of the faces of the octahedra below; conversely, the tetrahedral faces of the SiB tetrahedra are oriented in the opposite (O) direction from the faces of the octahedra to which they are connected; for additional illustration of S- and O-rotations, see Figure 7 of Cameron and Papike (1981).

rotated silicate chains in a tetrahedral layer has not been observed in any other pyroxene structure. The crystal structure of high-*P* protopyroxene has many similarities to that of orthopyroxene. For example, the SiO_4 tetrahedra in the less kinked chains in both structures were smaller but more distorted than those in the more kinked chains; moreover, the M1 octahedron was smaller in terms of both mean M-O bond length and octahedral volume and much less distorted than the M2 octahedron. In addition, the M2 octahedron shared only one O2-O3 edge with the adjacent tetrahedron. Based on the ideal structure model of regular tetrahedra and octahedra, Thompson (1970) and Papike et al. (1973) predicted the existence of the $P2_1cn$ protopyroxene structure consisting of both S- and O-rotated silicate chains. The high-*P* protopyroxene structure was determined here to possess all predicted features. From X-ray intensities measured from precession films taken on a protoenstatite crystal at 1100 °C, Smyth (1971) noted several reflections violating the *b*-glide symmetry and refined the structure based on the space group $P2_1cn$, which yielded $R_w = 0.18$ and $R = 0.23$ with some unpredicted structural features. Nevertheless, Smyth also noted the presence of significant stacking disorder in his sample and suggested that the violation of *b*-glide symmetry may have arisen from the stacking disorder. Further in-situ high-temperature investigations showed that stacking disorder in protoenstatite transformed from orthoenstatite at high temperatures is a common phenomenon and the true space group of protoenstatite should be *Pbcn* rather than $P2_1cn$ (Murakami et al. 1982; Yang and Ghose 1995a).

Within the experimental pressure range, both SiA and SiB tetrahedra behaved as rigid units: no significant variations were found in the mean Si-O bond lengths, tetrahedral volumes, or distortion indices. However, the O3-O3-O3 angles of two silicate chains decreased appreciably as pressure increased and the more kinked A chain showed a greater reduction (8.6°) between 2.50 and 9.98 GPa than the B chain (6.1°) (Table 3). The smaller change in the kinking angle of the B chain compared to the A chain as a function of pressure was due to the constraint imposed by the edge sharing between the SiB tetrahedron and the M2 octahedron.

Pressure affected the configurations of the two octahedra, especially M2: Both octahedra became considerably less distorted at higher pressures and their volumes varied linearly with pressure (Fig. 5). All individual M-O bond lengths within the M1 octahedron decreased as pressure increased, with the M1-O1B′ distance compressing most (4.1%) between 2.50 and 9.98 GPa and the M1-O2A length least (0.8%); the mean M1-O bond distance reduced by 2.0% in the same pressure range. Within the

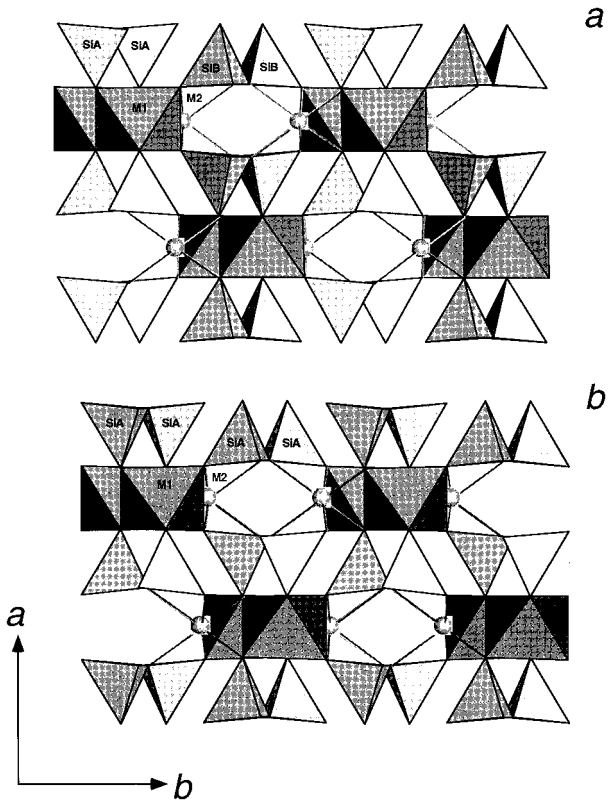

FIGURE 4. Crystal structure viewed along [001]: (**a**) high-*P* protopyroxene at 2.50 GPa and (**b**) low-*P* protopyroxene at 2.03 GPa. The SiA tetrahedral chains in high-pressure protopyroxene are S-rotated and the SiB chains O-rotated.

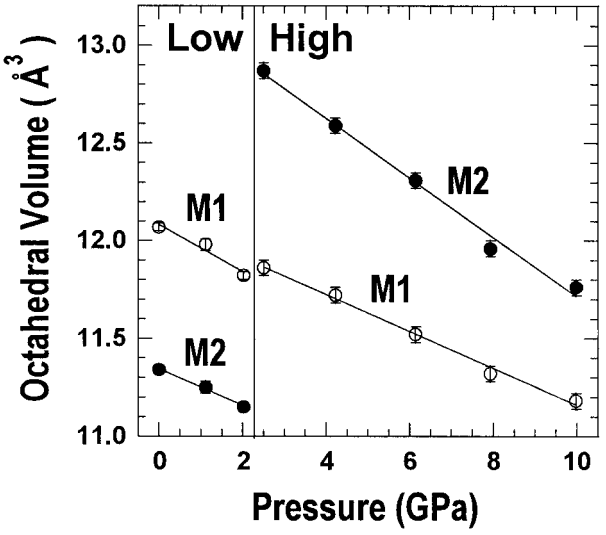

FIGURE 5. M1 and M2 octahedral volumes as a function of pressure.

M2 octahedron, while the M2-O1A and M2-O2B bond distances were virtually unchanged from 2.50 to 9.98 GPa, the two longest M2-O3A and M2-O3B bond distances shortened by as much as 10.8 and 4.7%, respectively, resulting in a substantial decrease in the mean M2-O bond length from 2.173 to 2.099 Å (3.4%) (Fig. 2). The shortening of the M2-O3 distances was directly related to the increased kinking of the A and B chains. The great compression of the M2-O3 bonds was not only responsible for the pronounced decrease in the degree of distortion of the M2 octahedron (Table 4) but also contributed most to the large compressibility of the mean M2-O bond length relative to the mean M1-O distance. The linear compressibilities of the mean M1-O and M2-O bond lengths were 0.0028(1) and 0.0046(2) GPa^{-1}, respectively, and the bulk moduli of the M1 and M2 octahedra were 128(6) and 87(5) GPa. This result should be compared with that for low-*P* protopyroxene in which the M2 octahedron was less compressible than the M1 octahedron.

High-pressure Raman spectra

Raman spectra of Li^{+}- and Sc^{3+}-doped protopyroxene were measured at ambient conditions by Mao et al. (1987) and Ghose et al. (1994). According to the calculations of Ghose et al. (1994), 60 Raman active modes exist in $MgSiO_3$ protoenstatite. In this study, 15 modes were observed under ambient conditions and a maximum of 12 modes in the diamond-anvil cell. Peak positions at ambient conditions were consistent with the observations of Mao et al. (1987) and Ghose et al. (1994), as well as with those observations made by Sharma (1989) from pure $MgSiO_3$ at high temperature. The Raman spectra obtained at 1.7, 2.5, 4.8, and 9.8 GPa are shown in Figure 6.

The most intense peak at all pressures studied was the symmetric, bridging Si-O stretch, initially at ~675 cm^{-1} at ambient pressure. This mode shifted continuously to higher frequencies with increasing pressure to 10.4 GPa. The behavior of the $Si\text{-}O_{br}$ mode across the phase transition in protopyroxene was quite different from that associated with the inversion from low- to high-*P* clinoenstatite in which an intense doublet in the $Si\text{-}O_{br}$ stretching region in the low-pressure form abruptly became a single peak after the phase transition (Chopelas and Boehler 1992). This behavior corresponded to the structural change in which two symmetrically distinct chains in low-*P* clinoenstatite became identical in the high-pressure form. In the transformation of protopyroxene to its high-*P* form, the opposite result occurred, that is, one type of silicate chain in low-*P* protopyroxene became two at the phase transition. Yet, no splitting of the narrow, intense peak into a doublet after the phase transition was observed. The reasons for this are unclear. Because the intensities of protopyroxene Raman peaks were sensitive to crystallographic orientation with respect to both incident and scattered light (Mao et al. 1987), further probing with different scattering angles may reveal a doublet of the symmetric $Si\text{-}O_{br}$ stretch for high-protopyroxene.

The non-bridging, asymmetric Si-O stretching doublet, initially at ~1050 cm^{-1} at ambient pressure, was broad and not resolvable as two individual peaks at pressures

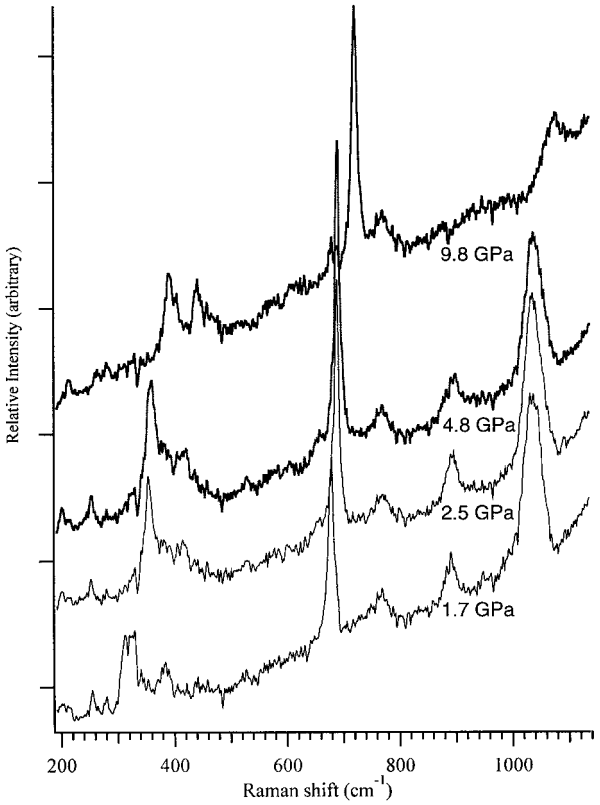

FIGURE 6. Raman spectra at of protopyroxene at four different pressures. The high-frequency limits of the spectra are imposed by the intense diamond peak at ~1332 cm^{-1}.

above 1 GPa in the diamond-anvil cell. As pressure increased, the peak position shifted continuously to higher frequencies, peak width increased, and peak intensity decreased.

A doublet of moderate strength at frequencies initially between 305 and 340 cm^{-1} at ambient pressure was present at pressures up to 1.7 GPa. Peaks around these frequencies described M1 and M2 cation translational movement, according to the computed partial density of states of all atoms in protoenstatite (Ghose et al. 1994). As pressure increased from 1.7 to 2.5 GPa, the doublet disappeared and a new mode appeared abruptly at 350 cm^{-1} (Fig. 6). This discontinuous change indicates a phase transition consistent with the X-ray diffraction data.

Structural changes associated with the *Pbcn*-to-*P*2_1*cn* phase transition

The most dramatic structural change involved the abrupt splitting of one type of O-rotated silicate chain in low-*P* protopyroxene into an S-rotated A and an O-rotated B chain in high-*P* protopyroxene, coupled with a marked decrease in the O3-O3-O3 angles and the re-configuration around the M2 site. The kinking angle of the silicate chain in low-*P* protopyroxene at 2.03 GPa was 165.9°, whereas it was 147.9° and 153.9° for the A and

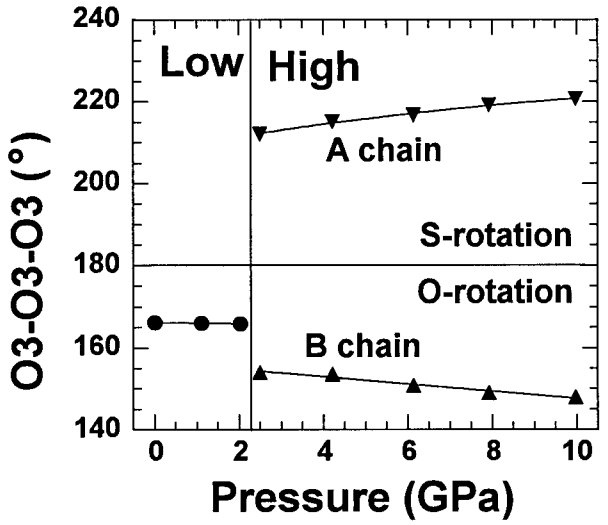

FIGURE 7. O3-O3-O3 kinking angles in protopyroxene as a function of pressure. The kinking angle of the S-rotated A chain is plotted as 360° minus the O3-O3-O3 angle in accordance with Sueno et al. (1976).

B chains, respectively, in high-*P* protopyroxene at 2.50 GPa (Fig. 7). The introduction of the S-rotated A chain and the increased kinking for both chains yielded an unusual coordination for the M2 site. The coordination of the M2 cation in low-*P* protopyroxene at 2.03 GPa could be considered as (4 + 2): two O1 and two O2 atoms at an average distance of 2.074 Å and two O3 atoms at 2.344 Å. However, it becomes a (4 + 1 + 1) configuration in high-*P* protopyroxene at 2.50 GPa; with O1A, O1B, O2A, and O2B at an average distance of 2.044 Å, O3B at 2.235 Å, and O3A at 2.632 Å. This change increases the M2 octahedral volume by as much as 15.4% and the mean M2-O bond distance by 0.4% (assuming a sixfold coordination for comparison). The high-*P* phase had considerably less efficient packing around the M2 site, which accounted for the increase in the compressibility of the M2 octahedron in high-*P* protopyroxene relative to that in low-*P* protopyroxene. The rearrangement about the M2 site actually involved a switching of the bridging O3 atoms coordinated to the M2 cation (Fig. 8). From 2.03 to 2.50 GPa, one of the M2-O3 lengths increased discontinuously from 2.344 to 2.961 Å; simultaneously, one of the M2-O3' lengths decreased from 3.512 to 2.632 Å. Due to this switching, the degree of distortion of the M2 octahedron was substantially reduced: the angle variance of the M2 octahedron was 342.9(8)° in low-*P* protopyroxene at 2.03 GPa but became 131.9(9)° in high-*P* protopyroxene at 2.50 GPa. The switching of the O3 atoms coordinated to M2 also eliminated edge sharing with the adjacent tetrahedron in the A chain in high-*P* protopyroxene.

The observed changes in unit-cell parameters across the phase transition were a direct consequence of the prominent structural modifications described above. The

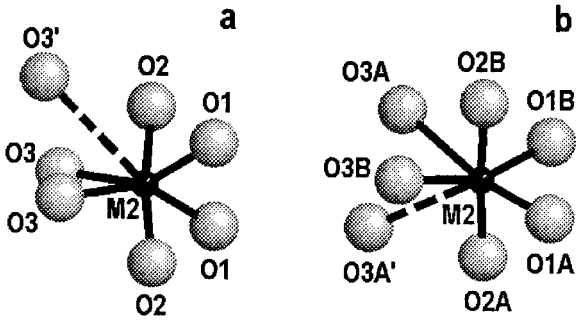

FIGURE 8. Atomic coordination for the M2 cation in (**a**) low-*P* protopyroxene at 2.03 GPa and (**b**) high-*P* protopyroxene at 2.50 GPa. The distances connected with solid lines are within 2.8 and the dashed lines beyond 2.8°.

2.4% reduction in the *c* dimension arose from the evident decrease in the O3-O3-O3 angles of the silicate chains, which ran parallel to the *c* axis in both low- and high-*P* protopyroxene structures. The sudden decrease in the O3-O3-O3 angles of the silicate chains, coupled with the change in the M2-O3 bond lengths, was also largely responsible for the increase in the *b* dimension, because the kinking or unkinking of tetrahedral chains in protopyroxene (and other pyroxenes as well) was principally confined in the *b*-*c* plane. The discontinuous shortening in the *a* dimension as pressure increased from 2.03 to 2.50 GPa, in contrast, was closely associated with the bond-distance changes in the M1 and M2 octahedra, as both low- and high-*P* protopyroxene structures were characterized by alternate stacking of layers of nearly rigid SiO_4 tetrahedra and relatively soft MO_6 octahedra along the *a* axis. The above arguments also led to the conclusion that the compression of both *Pbcn* and $P2_1cn$ protopyroxene structures along the *b* and *c* axes was controlled primarily by the high-pressure behavior of silicate chains, whereas the compression along the *a* axis was dominated by the compressibilities of MO_6 octahedra. As suggested above, a larger β_c value in pyroxene was associated with more kinked silicate chains. Accordingly, the more kinked silicate chains in high-*P* protopyroxene explained the noticeable increase in β_c and decrease in β_b across the *Pbcn*-to-$P2_1cn$ transformation. The greater compressibility of high-*P* protopyroxene stemmed from the increased freedom for atomic displacements in the structure and the much less efficient packing around the M2 site.

The *Pbcn*-$P2_1cn$ inversion in protopyroxene was reversible with an apparent hysteresis effect and is marked by discontinuous changes in all unit-cell dimensions and several structural parameters, such as the O3-O3-O3 angles of silicate chains, some M-O bond lengths, and the M2 octahedral distortion indices. Hence, it was a displacive first-order phase transition. Structurally, this transition was driven by the differential compression between SiO_4 tetrahedra and MO_6 octahedra. At high pressure, the SiO_4 tetrahedra in low-*P* protopyroxene acted as a nearly rigid unit, whereas the MO_6 octahedra were relatively soft. To reduce the misfit produced by this compressibility difference and maintain the *Pbcn* symmetry, the structure responded to pressure by increasing the kinking of silicate chains and the distortion of the M2 octahedron. However, the extent to which the silicate chains could kink and the M2 octahedron could distort was hindered by sharing of two O2-O3 edges in each extremely distorted M2 octahedron with SiO_4 tetrahedra in two adjacent silicate chains that were related by the *b*-glide symmetry. At the transition pressure, the simultaneous adjustment in the configuration of the two symmetrically related silicate chains could no longer match the change in the geometry of two octahedra, especially M2. Consequently, the *b*-glide symmetry broke to allow the independent modifications of two silicate chains, giving rise to the $P2_1cn$ structure.

Energetically, the stability of low-*P* protopyroxene was mainly affected by two factors: the interaction between Si^{4+} and M2 cations across the two shared O2-O3 edges and the local strain developed around the M2 octahedron due to its large distortion. In this sense, attainment of an energetically favorable configuration for the M2 cation was a primary driving force for the phase transition. At 2.03 GPa, two Si^{4+} cations were only 2.858 Å away from the M2 cation, and the angle variance of the M2 octahedron reached a value of 342.9, the largest value observed thus far among all pyroxenes at any conditions. As pressure was raised further, the local energy around the M2 site increased, due to the increased Si^{4+}-M2 repulsion and M2 octahedral distortion, such that the low-*P* protopyroxene structure could no longer accommodate it. The high-*P* protopyroxene structure thus resulted in which, due to the breaking of a M2-O3 bond and formation of a new one, only one M2-Si separation was within 3.0° and the *AV* value of the M2 octahedron decreased to 131.9 at 2.50 GPa.

All phase transitions in pyroxenes at high temperatures and pressures involve a change in the number of the O2-O3 edges shared between the M2 octahedron and adjacent SiO_4 tetrahedra. Phase transitions caused by increasing temperature were associated with an increase in this number from one to two, e.g., transformations from low- to high-pigeonite (Brown et al. 1972), low- to high-clinopyroxene (Smyth and Burnham 1972), orthoferrosilite to high-clinoferrosilite (Sueno et al. 1984), orthoenstatite to protoenstatite (Yang and Ghose 1995a), and Mg-rich orthopyroxene to a transitional state (Yang and Ghose 1995b). Phase transitions resulting from increasing pressure were associated with a decrease in the number of the shared O2-O3 edges, e.g., transformations from low- to high-*P* clinopyroxene (Angel et al. 1992; Hugh-Jones et al. 1994), orthoferrosilite to high-*P* clinoferrosilite (Hugh-Jones et al. 1996), and low- to high-*P* protopyroxene (this study). These observations suggest that interactions of Si^{4+}-M2 cations play a crucial role in the relative stability of a pyroxene structure. Accordingly, as an Si-M2 separation in high-*P* protopyroxene decreases con-

siderably from 2.745(5) Å at 2.50 GPa to 2.676(5) Å at 9.98 GPa, another structural change from high-*P* protopyroxene to a new phase can be postulated at even higher pressures to break up this unstable configuration. This means that the M2 octahedron in the new phase may not share any edge with adjacent SiO_4 tetrahedra. Such a configuration for the M2 cation has been found in high-*P* clinopyroxene (Angel et al. 1992; Hugh-Jones et al. 1994). This reasoning may also provide a crystal-chemical explanation as to why high-*P* clinopyroxene is the stable form of Ca-poor pyroxenes.

Conclusions

In addition to his prediction of the existence of the $P2_1cn$ protopyroxene structure, Thompson (1970) also suggested that the ideal space group for orthopyroxene should be $P2_1ca$, rather than *Pbca*, and both O- and S-rotated silicate chains should occur in the $P2_1ca$ structure. Because silicate chains in both low-*P* protopyroxene and orthopyroxene are all O-rotated, and both structures contain a parity violation in the tetrahedral layers, the discovery of the $P2_1cn$ protopyroxene structure implies the possible existence of $P2_1ca$ orthopyroxene at high pressures. However, Hugh-Jones and Angel (1994) did not detect such a transition in $MgSiO_3$ orthoenstatite up to a pressure of 8.5 GPa at room temperature. Thus, if the $P2_1ca$ phase can be made, it presumably will require a pressure higher than 8.5 GPa and/or a composition different from $MgSiO_3$. Furthermore, because great similarities exist between pyroxenes and amphiboles, phase transitions with shifts in chain orientation similar to that observed in protopyroxene may also exist in protoamphiboles and orthoamphiboles, as well as other pyriboles at high pressures.

Acknowledgments

X-ray diffraction work is supported by NSF grant EAR-9218845 and vibrational spectroscopy work by NSF EAR-9526763. Fellowships to H. Yang and P.G. Conrad at the Geophysical Laboratory are supported by the Center for High Pressure Research and by the Carnegie Institution of Washington.

References cited

Anderson, D.L. (1989) Theory of the Earth. Blackwell Scientific, Boston.

Angel, R.J. and Hugh-Jones, D.A. (1994) Equations of state and thermodynamic properties of enstatite pyroxenes. Journal of Geophysical Research, 99, 19777–19783.

Angel, R.J., Chopelas, A., and Ross, N.L. (1992) Stability of high-density clinoenstatite at upper-mantle pressures. Nature, 358, 322–324.

Becker, P.J. and Coppens, P. (1975) Extinction within the limit of validity of the Darwin transfer equations: III. Non-spherical crystals and anisotropy of extinction. Acta Crystallographica, A31, 417–425.

Brown, G.E., Prewitt, C.T., Papike, J.J., and Sueno, S. (1972) A comparison of the structures of low and high pigeonite. Journal of Geophysical Reseach, 77, 5778–5789.

Cameron, M. and Papike, J.J. (1981) Structural and chemical variations in pyroxenes. American Mineralogist, 66, 1–50.

Chopelas, A. and Boehler, R. (1992) Raman spectroscopy of high-pressure $MgSiO_3$ phases synthesized in a CO_2 laser heated diamond-anvil cell: perovskite and clinopyroxene. In M.H. Manghnani and Y. Syono, Eds., High Pressure Research: Application to Earth and Planetary Sciences, p. 101–108, Terra, Tokyo/AGU, Washington, D.C.

Finger, L.W. and King, H. (1978) A revised method of operation of the single-crystal diamond cell and refinement of the structure of NaCl at 32 kbar. American Mineralogist, 63, 337–342.

Finger, L.W. and Prince, E. (1975) A system of FORTRAN IV computer programs for crystal structure computations. National Bureau of Standards Technology Note 854.

Ghose, S., Choudhury, N., Chaplot, S.L., Pal Chowdbury, C., and Sharma, S.K. (1994) Lattice dynamics and Raman spectroscopy of protoenstatite $Mg_2Si_2O_6$. Physics and Chemistry of Minerals, 20, 469–477.

Hazen, R.M. and Finger, L.W. (1979) Polyhedral tilting: a common type of pure displacive phase transition and its relationship to analcite at high pressure. Phase Transitions, 1, 1–22.

———(1982) Comparative Crystal Chemistry. Wiley, New York.

———(1984) Compressibilities and high-pressure phase transitions of sodium tungstate perovskites (Na_xWO_3). Journal of Applied Physics, 56, 331–313.

———(1985) Crystals at high pressure. Scientific American, 252, 110–117.

Hugh-Jones, D.A. and Angel, R.J. (1994) A compressional study of $MgSiO_3$ orthoenstatite to 8.5 GPa. American Mineralogist, 79, 405–410.

Hugh-Jones, D.A., Woodland, A.B., and Angel, R.J. (1994) The structure of high pressure *C*2/*c* ferrosilite and crystal chemistry of high-pressure *C*2/*c* pyroxenes. American Mineralogist, 79, 1032–1041.

Hugh-Jones, D.A., Sharp, T., Angel, R.J., and Woodland, A.B. (1996) The transformation of orthoferrosilite to high-pressure *C*2/*c* clinoferrosilite at ambient temperature. European Journal of Mineralogy, 8, 1337–1345.

Hugh-Jones, D.A., Chopelas, A., and Angel, R.J. (1997) Tetrahedral compression in $(Mg,Fe)SiO_3$ orthopyroxenes. Physics and Chemistry of Minerals, 24, 301–310.

Ibers, J.A. and Hamilton, W.C., Eds. (1974) International tables for X-ray crystallography, vol. IV, 366 p. Kynoch, Birmingham, U.K.

Hahn, T., Ed., (1983) International Tables for Crystallography Volume A, Space-Group Symmetry, p. 224. Reidel, Dordrecht.

King, H.E. and Finger, L.W. (1979) Diffracted beam crystal centering and its application to high-pressure crystallography. Journal of Applied Crystallography, 12, 374–378.

Lehmann, M.S. and Larsen, F.K. (1974) A method for location of the peaks in step-scan-measured Bragg reflexions. Acta Crystallographica, A30, 580–584.

Mao, H.K., Xu, J., and Bell, P.M. (1986) Calibration of the ruby pressure gauge to 800 kbar under quasi-hydrostatic conditions. Journal of Geophysical Research, 91, 4673–4676.

Mao, H.K., Hemley, R.J., and Chao, E.C.T. (1987) The application of micro-Raman spectroscopy to analysis and identification of minerals in thin section. Scanning Microscopy, 1, 495–501.

Murakami, T., Takeuchi, Y., and Yamanaka, T. (1984) X-ray studies on protoenstatite: II. Effect of temperature on the structure up to near the incongruent melting point. Zeitschrift für Kristallographie, 166, 262–275.

———(1985) High-temperature crystallography of a protopyroxene. Zeitschrift für Kristallographie, 173, 87–96.

Pacalo, R.E.G. and Gasparik, T. (1990) Reversals of the orthoenstatite-clinoenstatite transition at high pressures and high temperatures. Journal of Geophysical Research, 95, 15853–15858.

Papike, J.J., Prewitt, C.T., Sueno, S., and Cameron, M. (1973) Pyroxenes: comparisons of real and ideal structural topologies. Zeitschrift für Kristallographie, 138, 254–273.

Ralph, R.L. and Ghose, S. (1980) Enstatite, $Mg_2Si_2O_6$: Compressibility and crystal structure at 21 kbar (abs.). EOS, 61, 409.

Ringwood, A.E. (1975) Composition and petrology of the Earth's mantle, p. 74–122. McGraw-Hill, New York.

Robinson, K., Gibbs, G.V., and Ribbe, P.H. (1971) Quadratic elongation: A quantitative measure of distortion in coordination polyhedra. Science, 172, 567–570.

Sadanaga, R., Okamura, F.P., and Takeda, H. (1969) X-ray study of the phase transformations of enstatite. Mineralogical Journal, 6, 110–130.

Sasaki, S., Prewitt, C.T., and Harlow, G.E. (1984) Alternative interpreta-

tion of diffraction patterns attributed to low ($P2_1ca$) orthopyroxene. American Mineralogist, 69, 1082–1089.

Sharma, S.K. (1989) Applications of advanced Raman spectroscopic techniques in Earth sciences. In H.D. Bist, J.R. Durig, and J.F. Sullivan, Eds., Vibrational spectra and structure, vol. 17B, p. 513–568. Elsevier, Amsterdam.

Smith, J.V. (1959) The crystal structure of protoenstatite, $MgSiO_3$. Acta Crystallographica, 12, 515–519.

———(1969) Crystal structure and stability of $MgSiO_3$ polymorphs: physical properties and phase relations of Mg,Fe pyroxenes. Mineralogical Society of America Special Paper, 2, 3–29.

Smyth, J.R. (1971) Protoenstatite: a crystal structure refinement at 1100 °C. Zeitschrift für Kristallographie, 134, 262–274.

———(1973) An orthopyroxene structure up to 850 °C. American Mineralogist, 58, 636–648.

———(1975) The synthesis and crystal structure of a magnesium-lithium-scandium protopyroxene. American Mineralogist, 62, 1252–1257.

Smyth, J.R. and Burnham, C.W. (1972) The crystal structure of high and low clinohypersthene. Earth and Planetary Science Letters, 14, 183–189.

Sueno, S., Cameron, M., and Prewitt, C.T. (1976) Orthoferrosilite: High-temperature crystal chemistry. American Mineralogist, 61, 38–53.

Sueno, S., Kitama, M., and Prewitt, C.T. (1984) The crystal structure of high clinoferrosilite. American Mineralogist, 69, 264–269.

Takuchi, Y. (1997) Tropochemical Cell-Twinning. Terra, Tokyo.

Thompson, J.B. (1970) Geometrical possibilities for amphibole structures: model biopyriboles. American Mineralogist, 55, 292–293.

Vaughan, M.T. and Bass, J.D. (1983) Single crystal elastic properties of protoenstatite: a comparison with orthoenstatite. Physics and Chemistry of Minerals, 10, 62–68.

Weidner, D.J., Wang, H., and Ito, J. (1978) Elasticity of orthoenstatite. Physics of the Earth and Planetary Interiors, 17, 7–13.

Woodland, A.B. and Angel, R.J. (1997) Reversal of the orthoferrosilite: high-P clinoferrosilite transition, a phase diagram for $FeSiO_3$ and implications for the mineralogy of the Earth's upper mantle. European Journal of Mineralogy, 9, 245–254.

Yang, H. and Ghose, S. (1995a) High-temperature single crystal X-ray diffraction studies of the ortho-proto phase transition in enstatite, $Mg_2Si_2O_6$, at 1360° K. Physics and Chemistry of Minerals, 22, 300–310.

———(1995b) A transitional structural state and anomalous Fe-Mg order-disorder in Mg-rich orthopyroxene, $(Mg_{0.75}Fe_{0.25})_2Si_2O_6$. American Mineralogist, 80, 9–20.

Manuscript received May 15, 1998
Manuscript accepted October 1, 1998
Paper handled by Anastasia Chopelas